NONLINEAR ULTRASOUND PROPAGATION IN WATER FROM SQUARE FOCUSED TRANSDUCER

TAMARA KUJAWSKA, JANUSZ WÓJCIK, ANDRZEJ NOWICKI

Institute of Fundamental Technological Research of Polish Academy of Sciences
Świętokrzyska 21, 00-049 Warsaw, POLAND
e-mail: tkujaw@ippt.gov.pl

The nonlinear pulsed acoustic pressure field from a focused square aperture is considered. Experimental measurements in water of a 4D sound field radiated from a 2.8 MHz focused square transducer of a 20 mm side and a 80 mm focal distance for excitation level producing an average acoustic pressure P_0 = 0.14 MPa at its surface are presented. The obtained results are compared with the numerical calculation results for the same boundary conditions. The novel, free from paraxial approximation and computationally efficient numerical algorithm was used to simulate the 4D nonlinear pulsed pressure field from the nonaxisymmetric acoustic source. Our theoretical model was based on the Time-Averaged Pressure Envelope (TAPE) method recently developed that enable to represent the propagated pulsed disturbance as a superposition of sinusoidal wavelets with carrier frequencies being the harmonics of the initial tone burst and with envelopes determined by the TAPE method. The novel approach to the solution of the nonlinear wave equation enabled to simulate full 4D nonlinear field for given boundary conditions in a dozen or so minutes utilizing the computational power of the standard PC.

INTRODUCTION

The theoretical and experimental studies of the finite amplitude acoustic waves propagation in attenuating media from nonaxisymmetric sources rather rarely can be found in literature in spite of the fact that probes of the rectangular geometry (such as linear phased arrays) are commonly used in clinical practice for medical ultrasonic imaging purposes. The main reason of such situation is a lack in simpler theoretical models and in computationally efficient numerical algorithms that are able to predict accurately the nonlinear effects in the 4D ultrasound field from pulsed arbitrarily shaped sources (plane and focused) in biological liquids and tissues with frequency-dependent absorption coefficients. Majority of previous models used to simulate the ultrasound beam propagation in lossy and nonlinear media are based on the KZK equation or it's expansion versions [5, 7, 8]. This model use a finite difference scheme required a large number of incremental steps to propagate the acoustic

wave forward with accounting for the effects of diffraction, absorption and nonlinearity over each step. The validity of this model is limited to the cases of plane or weakly focused acoustic beams (with slight diffraction effects) and to the paraxial area at the distance from the source equal to few it's radii. The numerical implementation of this model was developed only for axisymmetric sources and is known as the Bergen code.

The first, not restricted by the paraxial approximation theoretical model of the finite amplitude acoustic wave propagation in attenuating nonlinear media was developed by Christopher and Parker [3]. Their model used the incremental step scheme for the propagation of the acoustic wave forward and the operator-splitting method to account separately for the effects of full diffraction, arbitrary absorption and nonlinearity in acoustic beam over the small steps. The authors used the frequency-domain solution to the set of nonlinear wave propagation equations to account for the effects of diffraction and absorption for each spectral component as well as the time-domain solution to the Burgers equation of nonlinearity to account for the effects of nonlinear distortions. However the numerical implementation of the above model was developed only for a circular source geometry.

Tavakkoli *et al.* [4] have developed a time-domain numerical model capable to simulate the finite-amplitude focused acoustic pulse propagation in a dissipative and nonlinear medium. The model was used for predicting of pressure fields of highly focused sources developed for tissue destruction studies. It used a second order operator-splitting method with a fractional step scheme whereby the effects of full diffraction, arbitrary absorption and dispersion as well as nonlinearity were computed independently over fractional sub-steps. This model was more computationally efficient compared with the Christopher and Parker approach because the algorithm developed was able to use larger sub-steps in the beam propagation direction. The implementation of the model also was developed only for axisymmetric sources.

In recent years the only study describing the computationally efficient numerical model that is able to simulate accurately the 4D nonlinear ultrasound field in water and in biological tissues from pulsed nonaxisymmetric sources (including linear phased arrays) was developed by Zemp *et al.* [6]. Their model is based on the second order operator-splitting method proposed by Tavakkoli *et al*. with the modified fractional step scheme whereby the combined effects of diffraction and absorption are accounted for over half-steps and the effects of nonlinear harmonic interactions over full incremental steps. The computation of diffractive and absorption sub-steps was based on the angular spectrum technique with modified sampling method (to obtain computational savings due to larger axial propagation steps) while the computation of nonlinear steps was based on the time-domain solution to Burgers' equation. There are not reports yet describing an experimental confirmation of an agreement between the simulated pulsed nonlinear acoustic fields in water or in soft tissues from nonaxisymmetric focused sources (obtained by using the numerical model proposed) and nonlinear field from realistic probes.

In this work the experimental measurement results of the 4D nonlinear field from the square focused ultrasound transducer radiated the pulsed pressure wave in water are presented. The realistic beam patterns are compared with the simulation results obtained by using our novel numerical model. The proposed model is free from paraxial approximation, computationally efficient and capable of predicting the 4D ultrasound field in nonlinear and lossy media with arbitrary frequency-dependent absorption from pulsed, arbitrary shaped, plane and focused sources (including linear phased arrays with a beam deflection). Using the computational power of a standard PC the calculation time required for full 4D nonlinear field simulation by using our model depends on dimensions, the radiated frequency and the

excitation level of the source as well as on the absorption and nonlinearity strength of the medium and can vary from a few minutes to a few hours.

1. EXPERIMENT

Experimental measurements were made with a 2.8-MHz ultrasonic focused probe with a square aperture (of the sides a = 20 mm and the focal distance F = 80 mm) radiating in degassed distilled water. The pressure field generated by the transmitting transducer was measured using a wideband (calibrated over the range 1- 40 MHz) membrane PVDF hydrophone (Sonora Medical Inc. S/N S5-153, preamplifier P-159) with an active area of 0.414 mm in diameter. The probe was mounted on a translation stage driven by stepper motors allowing the transmitter motion in horizontal and vertical planes with given steps that could vary from 0.1 to 5 mm as well as rotation in azimuth. The transducer was driven by the pulse generator (model Ritec 1000) producing tone bursts of the variable level, frequency and duration. Measurements close to the transmitter surface (in order to determine the average pressure amplitude P_0 at the source being the input parameter to the numerical model) were made with short tone bursts (of 4 cycles duration) and measurements typically started at 4 cm from the transducer were realized with long tone bursts (of 8 cycles duration). Measurements were made along the acoustic beam axis Z, in both the XZ and YZ planes at the axial range from 40 mm to 120 mm with 5 mm steps and across the beam axis in the XY planes with 0.5 mm steps. The transverse plane measurements close to the transducer covered the square area corresponding to the range in both the X and Y directions equal to ± 15 mm as well as farther from the source – the area corresponding to the range ± 5 mm. The hydrophone was located on the acoustic beam axis by manual adjustment in the vertical and horizontal directions. The acoustic axis was determined from the symmetry of the beam (see Figs 1, 2). The hydrophone output was connected *via* linear broadband amplifier (model Ritec BR-640) to the input of an 8-bit digital oscilloscope (model HP54503A) with a 50 MHz sampling frequency. The received signals were digitized, averaged in the scope memory from 50 consecutive waveforms and sent to a PC *via* a GPIB interface for spectral analysis using FFT. Then the resulting harmonic components were corrected in agreement with the hydrophone sensitivity dependence on the frequency.

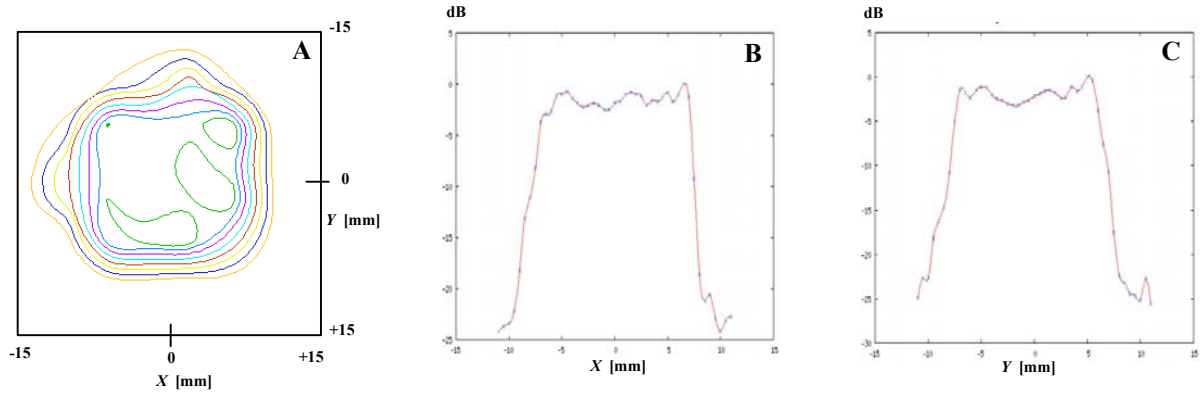

Fig.1 The measured transverse patterns of the acoustic pressure distribution close to the transducer at the distance z = 5 mm from the radiating surface: A) in the form of isobars (the range from – 2 dB to – 16 dB is shown) , B) along the X direction, C) along the Y direction

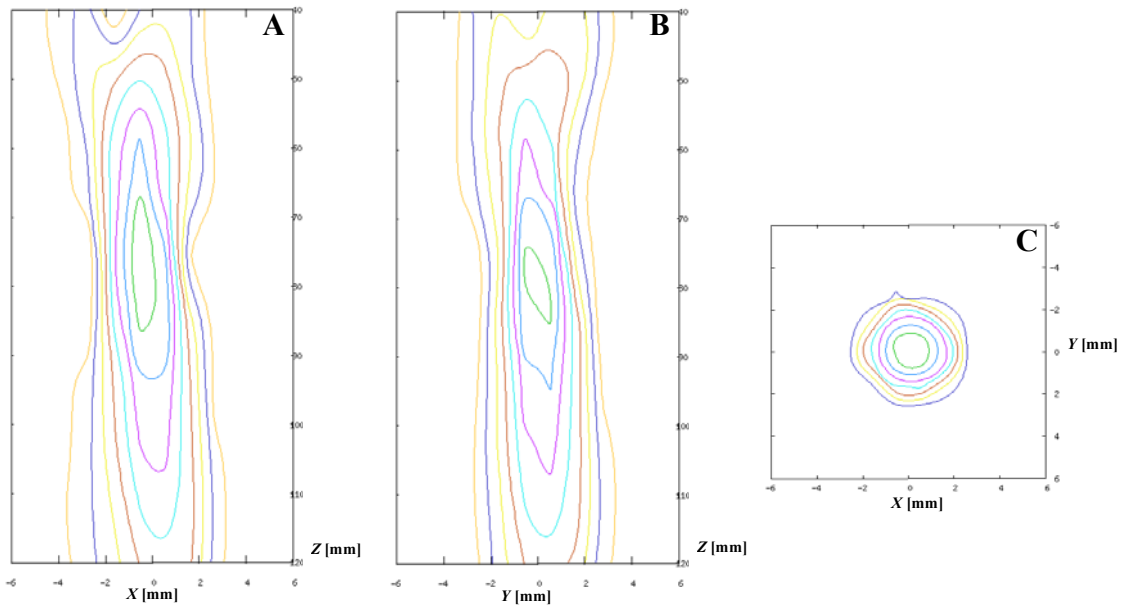

Fig.2 The measured acoustic field patterns visualized in order to ascertain the symmetry of the beam: A) and B) – in both the *XZ* and *YZ* axial planes, respectively and C) – in the *XY* plane at the distance z = 90 mm

In order to determine the average pressure amplitude P_0 at the source (required as the boundary condition parameter to the nonlinear numerical model) two sets of measurements were made: at low and high drive levels. The measured axial pressure distribution at the low drive level was compared with the numerical simulation results for given aperture dimensions and various P_0 values when linear theory was applied. In this case the contents of higher harmonics in the beam spectrum was inconsiderable and the propagation could be treated as a linear problem. The measured axial acoustic pressure that fitted the best to the calculated one provided the determination of P_0 value for the low drive level. The second set of measurements was made at the high drive level when the nonlinear effects in the pressure field are considerable. The increase in the axial pressure amplitude from the low to the high drive level gives a scaling factor for P_0. The value of P_0 for the nonlinear case was found as the value for the linear case multiplied by the ratio of the pressures measured close to the aperture when the respectively high and the low drive level were used. The average pressure at the source as the input parameter to the numerical algorithm for the nonlinear field simulation was determined as P_0 = 0.14 MPa.

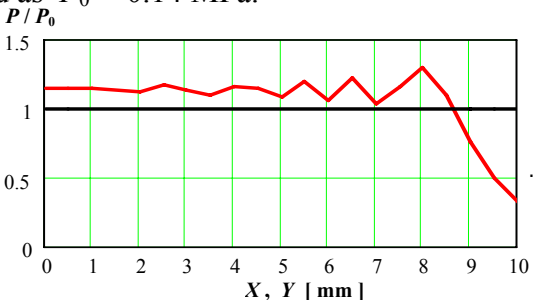

Fig.3 The normalized acoustic pressure distribution across the beam axis in both the *X* and *Y* directions assumed at the source surface (uniform) and calculated by using our numerical algorithm at the distance z = 5 mm from the source

The normalized uniform apodisation function at the source as the boundary condition to the numerical solution was assumed to be equal to 1. Then the calculated transverse pressure along the *X* and *Y* directions close to the source surface (at the distance z = 5 mm) has the distribution shown in Fig. 3. The agreement between both the calculated and measured transverse pressure distributions are very good (comparing with Figs 1B, 1C).

2. THEORETICAL MODEL

The model used to describe a propagation of an acoustic disturbance in a lossy and nonlinear medium is based on the equation [1] derived by the second author from the Kuznecov equation [2]. Our model provides the comprehensive near and far field description due to a linear hyperbolic operator (two first terms) describing the finite amplitude acoustic wave propagation as well as it is free from the paraxial approximation. In the dimensionless system of independent and dependent variables and retarded time this equation can be expressed as

$$\nabla^2 \mathrm{P} - 2\partial_{\tau z} \mathrm{P} - 2\partial_{\tau} \mathbf{A}\mathrm{P} = -\frac{P_0(\gamma+1)}{2\rho_0 c_0^2}\partial_{\tau\tau} \mathrm{P}^2, \qquad (1)$$

where $\mathrm{P} = \mathrm{P}(\mathbf{x}, z, \tau)$ is the dimensionless acoustic pressure; P_0 is the characteristic pressure (here the peak of the absolute pressure value at the source); ρ_0 and c_0 are the equilibrium density and sound velocity, respectively; γ is the exponent of the adiabate (for the empirical state equation $\gamma \equiv (B/A)+1$, where *B/A* is the non-linearity parameter of the medium); $\tau \equiv (t - z)$ denotes dimensionless retarded time; t is dimensionless time; $(\mathbf{x}, z)$ are dimensionless space coordinates (in the Cartesian coordinate system $\mathbf{x} \equiv (x, y)$, for axisymmetric sources in cylindrical coordinates $\mathbf{x} \equiv r$); $\nabla^2 \equiv \nabla_\perp^2 + \partial_{zz}$ is the Laplace operator, where $\nabla_\perp^2 \equiv \partial_{xx} + \partial_{yy}$ is the transverse component of the Laplacian (for parabolic approximation $\nabla^2 \cong \nabla_\perp^2$); A is the convolution-type operator describing an absorption ($\mathbf{A}\mathrm{P} \equiv A \otimes \mathrm{P}$, where $A = A(\tau)$ is a kernel of the operator A); a weak-signal absorption coefficient $a(n)$ is an eigenvalue of A with a corresponding eigenfunction $\exp(\pm i n \tau)$, n is the dimensionless frequency. Then $a = \mathrm{F}[A]$ where $\mathrm{F}[\cdot]$ is a Fourier transform with respect to time [1]. Equation (1) was normalized accordingly to:

$$\mathrm{P} \equiv \frac{P'}{P_0}; \quad \tau \equiv \Omega_0 \tau' = \Omega_0 \left(t' - z'/c_0\right); \quad (\mathbf{x}, z) \equiv K_0 \cdot (\mathbf{x}', z'); \quad n \equiv \frac{\omega'}{\Omega_0}$$
$$\nabla^2 \equiv \frac{1}{K_0^2}\nabla'^2; \quad \partial_\tau \equiv \frac{1}{\Omega_0}\partial_{\tau'}; \quad K_0 c_0 = \Omega_0, \qquad (2)$$

where $P'(\mathbf{x}', z', \tau')$ is the dimensional pressure; $(\mathbf{x}', z', t')$ are the dimensional coordinates and time; ω' is the angular frequency. The imposition of the relation $K_0 c_0 = \Omega_0$ causes the normalization of space and time in the same units. Both the distances and durations are measured in the number of wavelengths or cycles of the wave with the angular frequency Ω_0 multiplied by 2π. Assuming $K_0 = 2\pi/\lambda_0$, where λ_0 is the dimensional characteristic wavelength (here $\lambda_0 = d_0 + c_0 T'$, d_0 is the maximum distance between source points and T' is the initial disturbance duration), the corresponding dimensional time window for spectral analysis equals

to $T_0' = \lambda_0 / c_0$ and the condition of the separation of radiated periodic pulses in the half-space $z \geq 0$ is fulfilled. In the dimensionless units the windows (both the space and time) equal to 2π.

The solution $\mathrm{P}(\mathbf{x}, z, \tau)$ to Eq. (1) for a given boundary conditions was searched in the new form represented by a series *R* given by Eq. (3):

$$\mathrm{P} = \frac{1}{2}(R + R^*) \quad \text{where} \quad R(\mathbf{x}, z, \tau) \equiv \sum_{m=1}^{M} P_m(\mathbf{x}, z, \tau) e^{-i\, m\, \widetilde{N} \tau} + o^{M+1} \tag{3}$$

Here $\{P_m\}$, $m = 1, 2, ..., M$ describes the quasi-Fourier (quasi - because P_m depends also on time) spectrum of *R*. *M* is the effective dimension of the representation *R*. For $M = \infty$ the term $o^{M+1} \equiv 0$. $\widetilde{N}$ is the dimensionless carrier frequency of the boundary pulse (number of cycles with the period of $2\pi / \widetilde{N} \cdot \Omega_0$ contained in the window $T_0' = 2\pi / \Omega_0$), sign * denotes the complex conjugate. The disturbance is presented as the superposition of sinusoidal waves $P_m \exp(-i\, n_m \tau)$ bounded in time (wavelets) with the carrier frequencies $n_m = m\widetilde{N}$, which are the harmonics of the fundamental $\widetilde{N}$. The series (3) may be interpreted as the quasi-Fourier superposition of pulses with the envelopes P_m and the carrier frequencies n_m. Then the Fourier spectrum of the disturbance P can be represented by the superposition of the Fourier spectra of the *M* wavelets.

After substitution of Eq. (3) into Eq. (1) the following set of *M* equations for the envelopes P_m is obtained

$$\frac{1}{2 i m \widetilde{N}\, \vartheta_\tau^m} \nabla^2 P_m + \partial_z P_m + \bar{a}(m\widetilde{N}, \partial_\tau) P_m + \frac{1}{4} q i m \widetilde{N}\, \vartheta_\tau^m \prod_{m,l} P_l = 0, \quad m = 1, 2, \ldots, M \tag{4}$$

where $$\prod_{m,l} P_l = \sum_{l=1}^{m-1} P_{m-l} P_l + 2 \sum_{l=m+1}^{M} P_{l-m}^* P_l\,; \quad \vartheta_\tau^m \equiv \left(1 - \frac{\partial_\tau}{i m \widetilde{N}}\right); \quad q = \frac{P_0(\gamma + 1)}{2 \rho_0 c_0^2} \tag{5}$$

This set of equations is solved by using incremental propagation scheme and operator-splitting technique allowing to propagate linear and nonlinear effects separately over incremental steps. The nonlinear step consists in solving of the following equation

$$\partial_z P_m + \frac{1}{4} q i m \widetilde{N}\, \vartheta_\tau^m \prod_{m,l} P_l = 0, \quad m = 1, 2, \ldots, M \tag{6}$$

From the boundary conditions obtained from the solution of Eq. (6) the step accounting for the effects of both the full diffraction and arbitrary absorption consists in solving of the equation

$$\nabla^2 P_m + 2 i m \widetilde{N}\, \vartheta_\tau^m \left(\partial_z P_m + \left\{\bar{a}(m\widetilde{N}, \partial_\tau) P_m\right\}\right) = 0, \tag{7}$$

The determination of the envelope functions P_m for given boundary conditions to the nonlinear propagation model is based on P_m presentation as the product of the envelope function $P_L(\mathbf{x}, z, \tau)$ of the disturbance being the solution of the linear case (q = 0) of Eq. (1) for the same boundary conditions and functions $D_m(\mathbf{x}, z)$. Then the problem resolves to the

determination of $D_m(\mathbf{x}, z)$ functions. The indirect Time-Averaged Pressure Envelope (TAPE) method for determination of the set of M functions $D_m(\mathbf{x}, z)$ was used.

Our novel TAPE method enabled to shorten computational time of the full 4D nonlinear field simulation by several orders of magnitude allowing to predict nonlinear beam from rectangular focused apertures in less than 1 hour using the computational power the only standard PC.

3. RESULTS AND DISCUSSION

Figures 4–6 compare measurement results with theoretical predictions for square aperture tested. In all cases the experimental results are plotted as circle points and the numerical simulations as solid lines. The following boundary condition parameters were used in the calculations: c_0 = 1492 m/s, ρ_0 = 997 kg/m^3, B/A = 5.2, $\alpha = 2.8 \cdot 10^{-14}$ Np/(m·Hz^2). Fig. 4 shows both the calculated by our numerical solver and measured axial pressure amplitudes for the fundamental, 2-nd and 3-rd harmonic components.

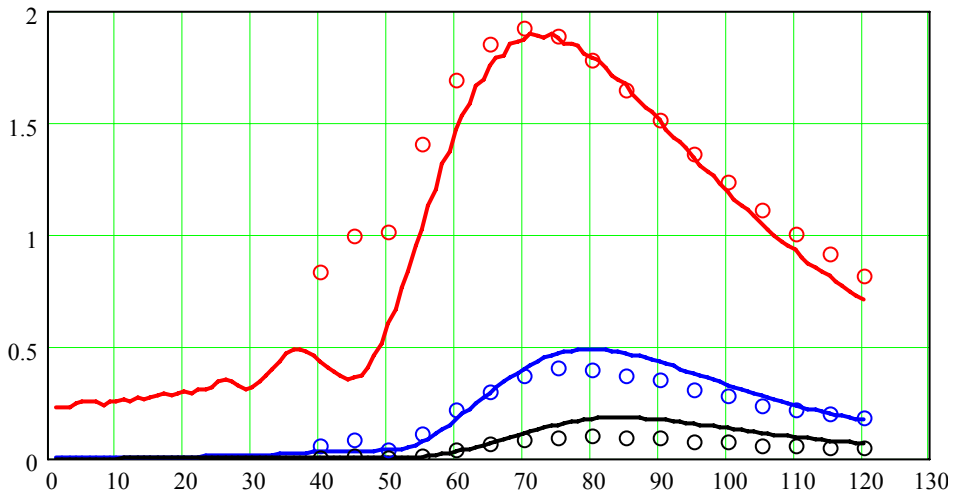

Fig.4 The 1-st (red), the 2-nd (blu) and the 3-rd (black) harmonic axial pressure distribution calculated by our numerical code (solid lines) and measured (points)

The agreement between experimental and numerical results for the square aperture is fairly good. The positions of the maxima are predicted accurately in spite of some discrepancies in amplitudes. A number of factors could be responsible for this. The discrepancies may be caused by spatial averaging at the hydrophone or ‘strabismus’ of the transducer. It is also possible that the apodisation function in the concave plane of the square radiating aperture is not uniform as was assumed in the numerical algorithm. Fig. 5 shows on-axis acoustic pressure waveforms simulated by our numerical code and measured for the investigated square aperture radiated the initial average pressure of 0.14 MPa.

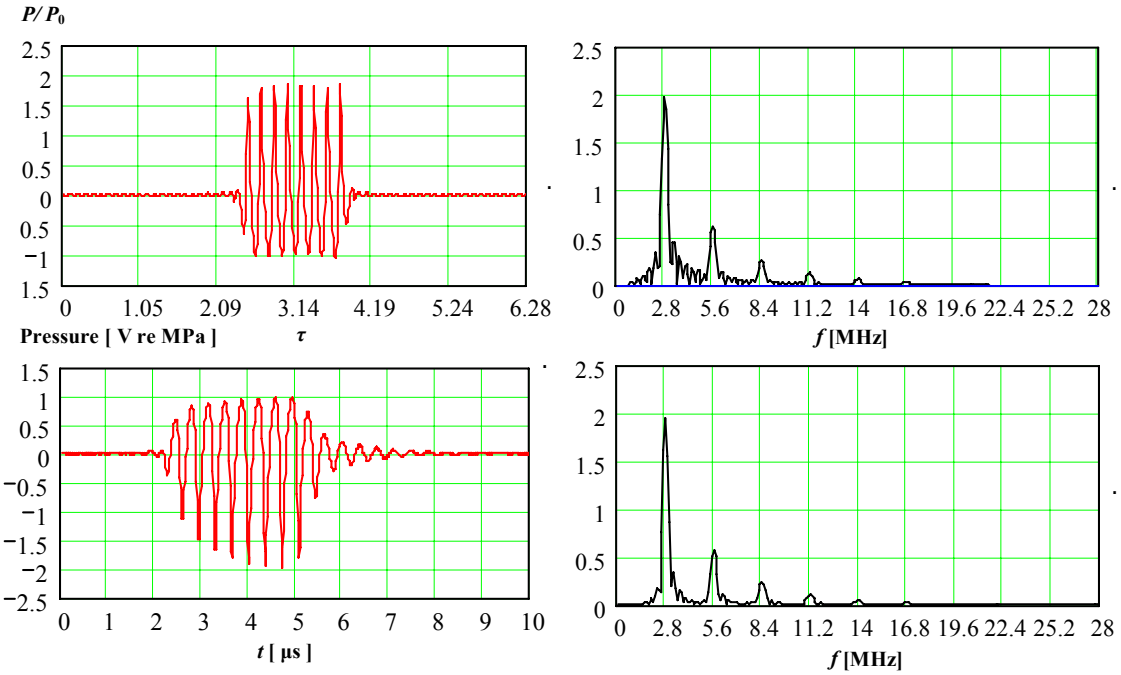

Fig.5 The normalized axial acoustic pressure waveform at the focal distance z = 80 mm calculated by our numerical solver (left top) and measured (left bottom) for tested square focus transducer and their spectra, respectively

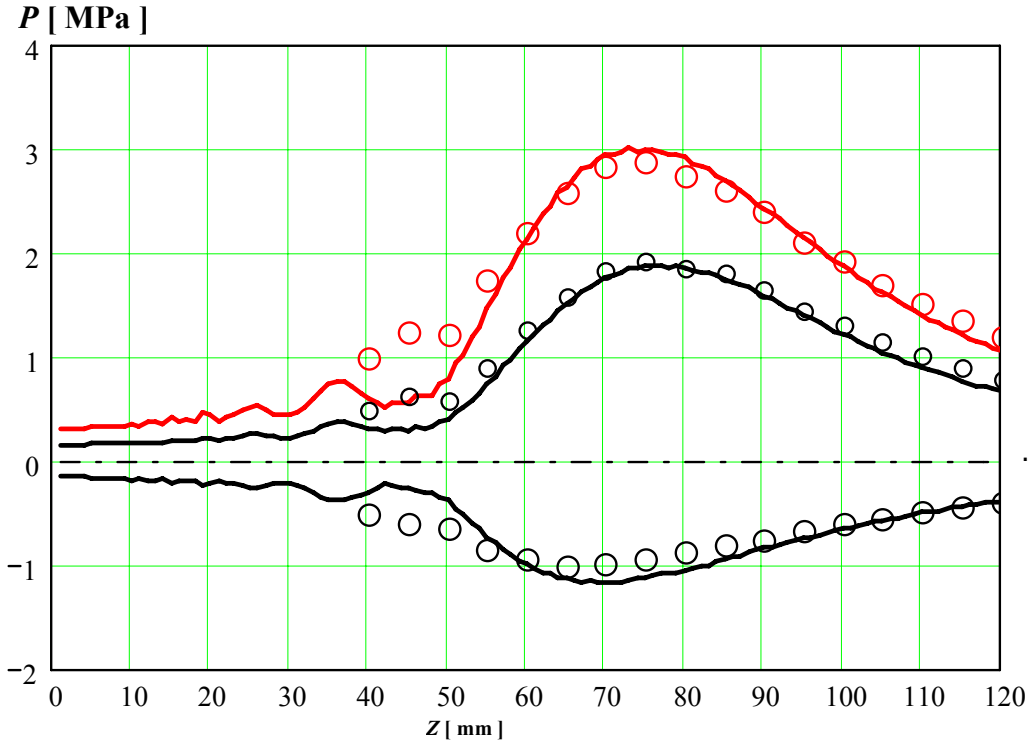

Fig.6 The peak-compression (top black), peak-rarefaction (bottom black) and peak-to-peak (red) axial pressure distributions calculated (lines) and measured (points) for initial pressure amplitude P_0 = 0.14 MPa

The measured transverse pressure distribution plots for the *X* and *Y* directions at the focal distance of 80 mm are demonstrated in Fig. 7.

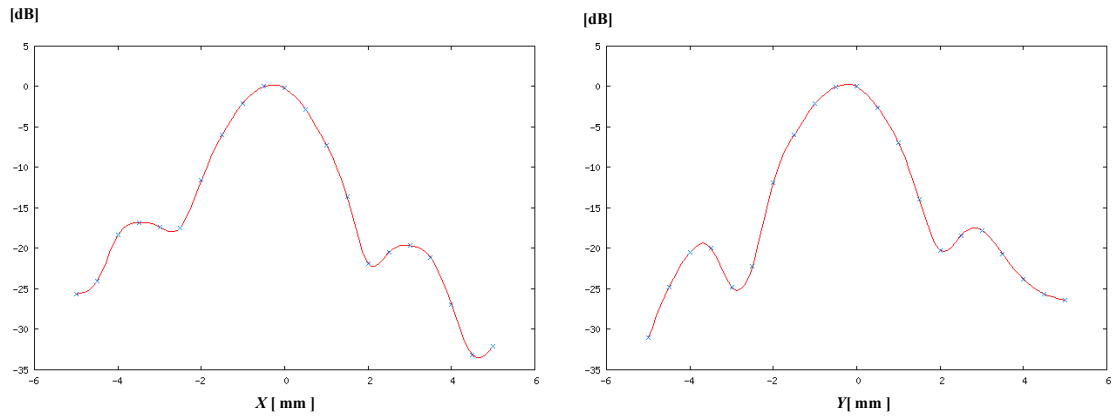

Fig.7 Transverse pressure distribution measured in the *X* and *Y* directions at the focal distance

The fundamental and 2-nd harmonic component pressure field in form of the logarithmic scale isobar plots filled with color are illustrated in Fig. 8.

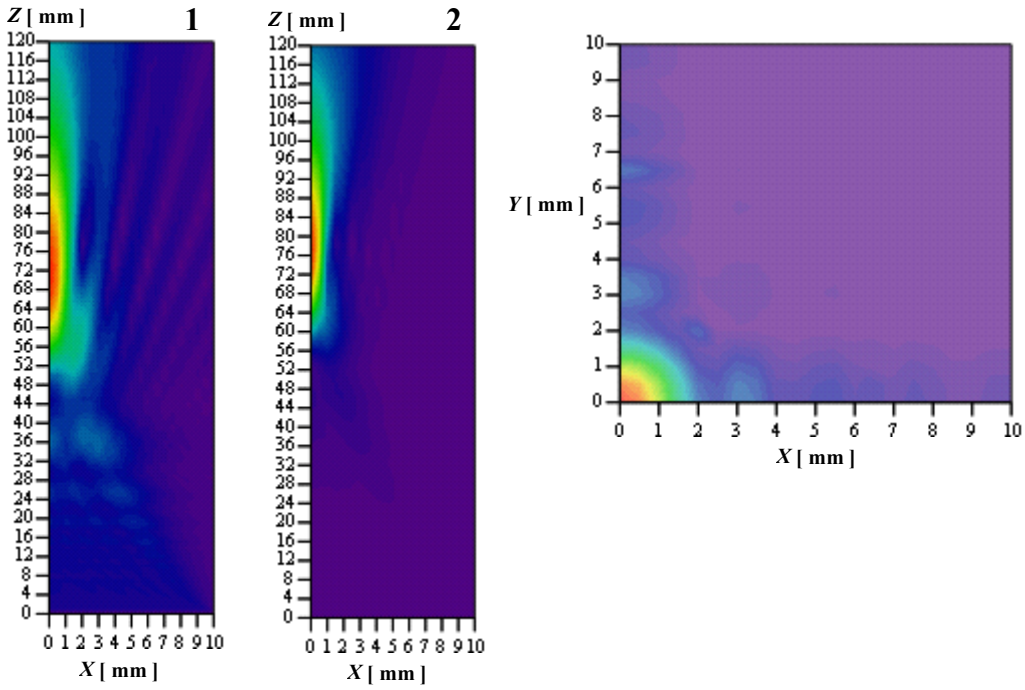

Fig.8 The fundamental and 2-nd harmonic component pressure field in the *XZ* half-plane (left) and the transverse peak-to-peak pressure field in the focal plane

4. CONCLUSIONS

Measurements of the acoustic pressure field from square focused aperture were presented. Two different levels of pulsed excitation corresponding to linear and nonlinear cases of sound propagation were applied to determine accurately the average pressure

amplitude at the source that is required as the input parameter for our numerical algorithm. Comparison between experimental and numerical simulation results has shown that our numerical code, based on the Time-Averaged Pressure Envelope (TAPE) method, predicts well the structure of the ultrasound field for considered boundary conditions.

ACKNOWLEDGEMENTS

Financial support from the National Committee of Scientific Research is acknowledged (Grant Nr 5T07B00924).

REFERENCES

[1] J. Wójcik, Conservation of energy and absorption in acoustic fields for linear and nonlinear propagation, J. Acoust. Soc. Am. **104**, 2654-2663, 1998.
[2] V. P. Kuznetsov, Equations of nonlinear acoustics, Akust. Zh. **16**, 548-553, 1970.
[3] P. Christopher, K. Parker, New approaches to nonlinear diffractive field propagation, J. Acoust. Soc. Am. **90**, 488-499, 1991.
[4] J. Tavakkoli, D. Cathignol, R. Souchon, O. A. Sapozhnikov, Modelling of pulsed finite-amplitude focused sound beams in time domain, J. Acoust. Soc. Am. **104**, 2061- 2072, 1998.
[5] A. C. Baker, A. M. Berg, A. Sahin, J. N. Tjøta, The nonlinear pressure field of plane, rectangular apertures: Experimental and theoretical results, J. Acoust. Soc. Am. **97**, 3510-3518, 1995.
[6] R. J. Zemp, J. Tavakkoli, R. S. C. Cobbold, Modeling of nonlinear ultrasound propagation in tissue from array transducers, J. Acoust. Soc. Am. **113**, 139-152, 2003.
[7] M. D. Cahill, A. C. Baker, Numerical simulation of the acoustic field of a phased array medical ultrasound scanner, J. Acoust. Soc. Am. **104**, 1274-1283, 1998.
[8] M. D. Cahill, A. C. Baker, Increased off-axis energy deposition due to diffraction and nonlinear propagation of ultrasound from rectangular sources, J. Acoust. Soc. Am. **102**, 199-203, 1997.